

Communication

A Compact Metamaterial-Based Antenna for Multiband Phased Array Applications

Diego Gallardo¹, David Monasterio¹, Ricardo Finger, F. Patricio Mena², and Leonardo Bronfman¹

Abstract—In this communication, we present a miniaturized multiband metamaterial (MTM)-based antenna for array applications, operating with good radiation performance over the long term evolution (LTE) and Universal Mobile Telecommunications System (UMTS) uplinks within the 800–3000 MHz range. Each antenna element consists of a radiator and an MTM reflector. The former is a miniaturized Archimedean spiral antenna with an integrated matching line. The latter is placed 39 mm below the radiator and is shared among the multiple elements in the array application. The radiator is very compact, a square of 75 mm per side, equivalent to only 0.2 (0.75) times the free-space wavelength at 800 MHz (3000 MHz). The reflector is incorporated to achieve half-space radiation and is implemented with a novel multilayered MTM structure to improve the radiation efficiency. The MTM, moreover, is used in a nonconventional way. In fact, we take advantage of its complete phase-response function, behaving, thus, as a magnetic or electric conductor in different parts of the band. In this way, the in-phase reflection is not limited by the typical narrow bandwidth of artificial magnetic conductors. The measured S_{11} parameter is less than -8 dB and the simulated gain is greater than 4.2 dBi in a range exceeding the one covered by the UMTS and LTE uplinks. Furthermore, a 2×2 antenna array was also built. The reflections of each element are similar to those obtained in the single-element antenna.

Index Terms—Antenna arrays, antennas, broadband antennas, metasurface, multifrequency antennas.

I. INTRODUCTION

Multiband and broadband antennas are useful for a diversity of applications, such as mobile telecommunications and some commercial applications [1]. Among all these applications, antenna arrays constitute one of the most widely used technologies, as they can achieve properties that no single antenna possesses. Although some implementations of multiband characteristics rely on the use of several narrowband antenna arrays, they imply more complicated hardware and also require more space. For this reason, multiband applications where the amount of hardware or space is limited must use arrays composed of single-element multiband antennas.

Many types of antennas could be used to form a multiband array. Examples are spiral [2], Vivaldi [3], and ultrawideband (UWB) monopole antennas [4]. However, the size of these antennas is

prohibitive for multiband arrays due to the generation of grating lobes at higher frequencies [5]. Even though miniaturization techniques could help to reduce the size of an antenna, they have an important limitation. The greater the miniaturization, the greater the decrease in radiation efficiency and impedance bandwidth [6]. In this sense, Archimedean spirals are good candidates given their ease of miniaturization [7], [8].

One problem with spiral antennas is that their radiation patterns cover all the space, causing an ambiguity in the synthesized beam of 2-D arrays. A possible solution is incorporating a common conductive reflector at a distance of $\lambda/4$ from the radiator (with λ the wavelength at the design frequency). However, this solution imposes a frequency dependence that could degrade the multiband operation [9]. In order to overcome this degradation, we propose using a metamaterial (MTM) reflector in a nonconventional way, instead.

The use of MTM reflectors has been widely studied [9]–[13]. In particular, spiral antennas integrated with MTM reflectors have been investigated in [14] and [15]. In all these applications, however, the MTM is used just as an artificial magnetic conductor (AMC), providing a phase shift ranging from $-\pi/2$ to $\pi/2$ in the reflected wave. For this reason, the antenna has to be placed close to the reflector and, although it could provide a low profile, it implies a bandwidth reduction since the MTM behaves as an AMC in a limited bandwidth. In this work, we propose a novel approach. The MTM is designed in such a way that its entire phase response is used, behaving, thus, as AMC or electrical conductor (EC) in different parts of the band. Without this approach, it is not possible to achieve half-space radiation with high radiation efficiency in the entire bandwidth of the radiator. Both, the novel MTM reflector and the very small electrical size of the radiator are required for this antenna to be useful for wide-angle phased arrays.

In this communication, we incorporate and optimize several techniques—antenna miniaturization, impedance matching, and MTM design—to achieve an MTM-based Archimedean spiral antenna, allowing multiband operation with a single port connection. Moreover, this antenna has a reduced size for array applications and a half-space directional pattern over the 800–1100 MHz and 1300–3000 MHz bands. Although these characteristics have been achieved individually, there is no antenna yet that satisfies them all simultaneously. The antenna presented here is intended to be used in the area of mobile telecommunications. Specifically, it has been designed for the uplinks of the Universal Mobile Telecommunications System (UMTS) and long-term evolution (LTE) bands centered at 750, 850, 900, 1700, 1900, and 2600 MHz, whose minimum and maximum frequencies are 703 and 2570 MHz. Due to its good radiation performance, half-space directional pattern, and small size, this antenna can be used to cover all the aforementioned uplinks in wide-angle phased arrays. To demonstrate its good performance in arrays, we have built and characterized a 2×2 array.

Manuscript received November 25, 2020; revised May 25, 2021; accepted May 27, 2021. Date of publication June 25, 2021; date of current version December 16, 2021. This work was supported by the Chilean National Commission for Scientific and Technological Research (CONICYT-ANID) under Grant Basal AFB-170002, Grant ALMA 31180005, and Grant Fondecyt 1180700. (Corresponding author: Diego Gallardo.)

Diego Gallardo and David Monasterio are with the Department of Electrical Engineering, Universidad de Chile, Santiago 8370451, Chile (e-mail: diego.gallardo@raig.uchile.cl; david.monasterio@raig.uchile.cl).

Ricardo Finger and Leonardo Bronfman are with the Department of Astronomy, Universidad de Chile, Santiago 8370451, Chile (e-mail: rfinger@u.uchile.cl; leo@das.uchile.cl).

F. Patricio Mena was with the Department of Electrical Engineering, Universidad de Chile, Santiago 8370451, Chile. He is now with the National Radio Astronomy Observatory, Charlottesville, VA 22903 USA (e-mail: fpmena@uchile.cl).

Color versions of one or more figures in this communication are available at <https://doi.org/10.1109/TAP.2021.3090861>.

Digital Object Identifier 10.1109/TAP.2021.3090861

0018-926X © 2021 IEEE. Personal use is permitted, but republication/redistribution requires IEEE permission.

See <https://www.ieee.org/publications/rights/index.html> for more information.

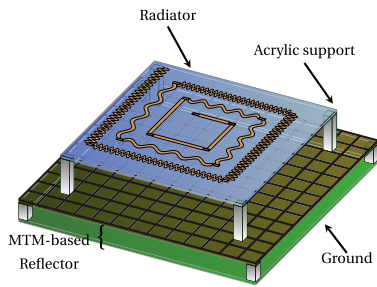


Fig. 1. Global scheme of the proposed antenna. The acrylic posts serve as mechanical supports. Only one arm of the spiral is shown (the other is patterned on the bottom side of the radiator's substrate).

II. ANTENNA STRUCTURE

The antenna consists of two parts, radiator and MTM reflector (Fig. 1). The radiator is a two-armed miniaturized Archimedean spiral antenna, that allows obtaining broadband characteristics. The reflector consists of a capacitive metasurface, separated by an air gap from a grounded dielectric.

A. Two-Armed Archimedean Spiral Antenna

The two-armed Archimedean spiral antenna is one of the most popular types of broadband antennas. Stable impedance and constant radiation pattern over multidecade frequency ranges are two of its most important characteristics. There are three regions in an Archimedean spiral antenna: transmission line (TL), radiation, and extinction regions [2], [5]. If λ_g is the guided wavelength, the radiation region occurs in a loop of radius $R_s = \lambda_g/2\pi$ and in a loop with side $L_s = \lambda_g/4$ in circular and rectangular spirals, respectively. The radiation zone of both types of spirals depends on λ_g and, hence, on the operation frequency. Moreover, the total size of the spiral defines its minimum operation frequency, while the size and shape of the inner loops define its maximum operation frequency. We have selected the rectangular shape since we want to decrease the overall size of the radiator (L_s for the rectangular spiral and $2R_s$ for the circular one) for a fixed frequency. Additionally, we have incorporated meandered lines to further miniaturize the design [6], [8].

B. MTM-Based Reflector

The use of an EC reflector limits to 100% the maximum fractional bandwidth that the radiator can achieve [16]. To overcome this limitation, we propose the use of an MTM reflector in a nonconventional way. MTMs are generally used as AMCs, which occur in reduced bandwidth, limiting the fractional bandwidth of the radiator. To solve this problem, we have designed an MTM that operates as an EC in the higher part of the operating band while it incorporates an *ad hoc* phase shift in the lower band.

The working principle of a reflector placed in the backside of an isotropic radiator is shown in Fig. 2. To obtain constructive interference, s_1 and s_2 must have a phase shift between $-\pi/2$ and $\pi/2$. Now, let us consider the phase shift of the MTM, described by a function $\Phi(f)$ of the frequency. Thereupon, the condition for constructive interference is defined as

$$-\pi/2 < -4\pi fd/c + \Phi(f) < \pi/2. \quad (1)$$

Equation (1) gives constraints for the values of Φ and, therefore, constitutes a guideline for the design of the MTM. For this work, we aim for an MTM that behaves as an EC in the frequency range

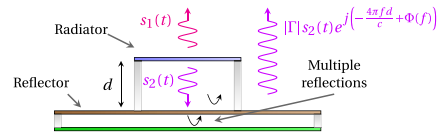


Fig. 2. Side view of Fig. 1, describing the effects of a reflector. d is the distance between the radiator and the reflector, $s_1(t)$ and $s_2(t)$ are the signals radiated by the radiator in the broadside directions and Γ is the reflection coefficient of the reflector. The idea is to reflect s_2 (thus causing half-space radiation) in such a way that it interferes constructively with s_1 (thus causing high radiation efficiency).

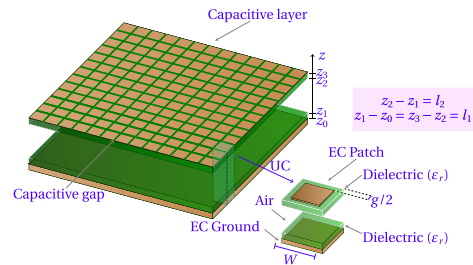


Fig. 3. Proposed MTM along with its UC.

of 950–2850 MHz, while incorporates an *ad hoc* phase shift from 700 to 950 MHz. Considering the stricter condition $\pm\pi/4$ for the limits of constructive interference, and taking $d = 39$ mm and $f = 950$ MHz as a representative frequency of the range 700–950 MHz, we conclude that Φ should be between 45° and 135° in this frequency band.

Once the constraints of the MTM reflector have been specified, we can proceed with its design. One of the best-known MTMs that could be useful for this work is the *mushroom-like* structure [9]. Although this structure satisfies some properties that are required for this work, it has some disadvantages, such as its narrow fractional bandwidth and its big size. Specifically, we require a fractional bandwidth of 26.18% (for the uplinks of the 750, 850, and 950 MHz bands, which cover the range of 703–915 MHz), but a mushroom-like structure can only achieve under 10%. Moreover, for operation at 703–915 MHz, the unit cell (UC) size of the mushroom-like structure is comparable to the desired size of the radiator. For these reasons, we propose a new design based on a variation of the mushroom-like structure, which is presented in Fig. 3. The idea behind this design is that it allows the replacement of the inductive via of the mushroom-like structure by a multiple-layer gap. Indeed, a conductive ground laminate viewed at a distance of less than $\lambda/4$ has an inductive impedance. This not only allows us to replace the via but also to increase the inductance value by properly adjusting the length of the multiple layers (hence, decreasing the operating frequency without increasing the lateral size W). As shown in [17], the multilayered structure also provides a fractional bandwidth larger than the one provided by the mushroom-like structure using the same commercially available substrates. However, it has the disadvantage that it allows surface waves to propagate since it has no vias to impede their propagation.

III. DESIGN AND SIMULATION

A. Radiator

The radiator was designed to be printed on a Rogers (TM) Kappa438 substrate ($\epsilon_r = 4.38$ and $\tan \delta = 0.005$) with a thickness of 1.5 mm. It is made up of two parts, a matching line and the Archimedean spiral itself. Both structures were implemented in

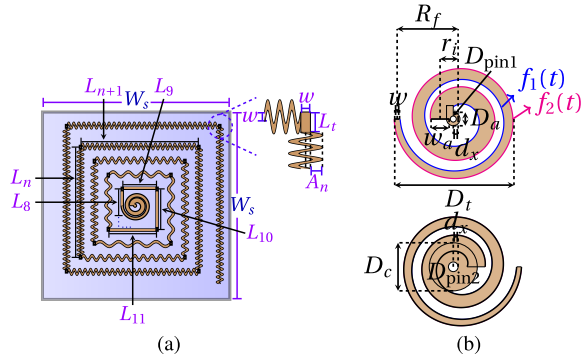


Fig. 4. Design of the rectangular spiral integrated with the matching line. (a) Line $n+1$ begins at the end of the line n and has a straight length of L_{n+1} . Lines 1 to 7 have been replaced by the matching line. There are five regions in the spiral. The first zone is made up of lines 8 to 11, the second zone is made up of lines 12 to 15, and so on. (b) Top and bottom view of the matching line.

TABLE I
GEOMETRIC PARAMETERS OF RADIATOR AND UC OF THE MTM

Spiral		Matching Line	
Parameter	Value	Parameter	Value
h_s	1.5 mm	r_i	3 mm
W_s	75 mm	w_a	3 mm
w	0.8 mm	d_x	0.74 mm
A_n	1 mm	D_{pin1}	1.4 mm
L_t	1.8 mm	D_{pin2}	2.9 mm
L_1	1.42 mm	D_a	2 mm
$L_{n>1}$	$2(n-1)L_1$	D_c	8 mm
N_I	0	R_f	9.94 mm
N_{II}	4	D_t	20 mm
N_{III}	12	$f_1(t)$	$r_i - w_a/2 + a_1 t$
N_{IV}	48	$f_2(t)$	$r_i + w_a/2 + a_2 t$
N_V	50	a_1	$(R_f - w/2 + w_a/2 - r_i)/(4\pi)$
-	-	a_2	$(R_f + w/2 - w_a/2 - r_i)/(4\pi)$

MTM unit cell			
Parameter	Value (mm)	Parameter	Value (mm)
L_1	0.96	L_5	0.73
L_2	1.92	L_6	1.46
L_3	3.84	L_7	2.92
L_4	5.1	L_8	3.85
w_1	0.66	w_2	0.53
s_1	0.2	s_2	0.075
a	5.5	b	2.655
c	7.02	p	20
l_s	4	w_s	0.7
p_s	4.9	-	-

Suffixes I to V refer to the five zones of the spiral. t is the angle of the cylindrical coordinates.

a balanced TL, which consists of two strips printed on the opposite faces of the dielectric substrate. For the design of the Archimedean spiral itself, we have to note that its radiation zone changes with frequency. Since we want to decrease the minimum operating frequency, we should prioritize the miniaturization in the outer section by adding more periods in the meandered lines. Taking this into consideration, we have divided the spiral into five zones and we have implemented meandered lines with different periods in each zone (N_I to N_V , given in Table I), as shown in Fig. 4(a).

To obtain a 50Ω impedance, we have implemented a matching line within the very spiral, as in [18]. The design of the matching line is shown in Fig. 4(b), and its parameters are given in Table I.

B. MTM Reflector

The basic structure of the MTM reflector was presented in Section II-B, considering the use of FR4 as substrate ($\epsilon_r = 4.4$ and $\tan \delta = 0.02$) with a thickness $l_1 = 1.5$ mm. The structure

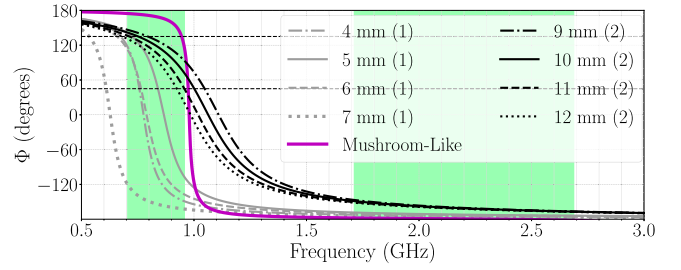


Fig. 5. Simulated phase of the S_{11} parameter of the MTM alone when using the initial (Fig. 3) and modified (Fig. 6) designs. The curves were obtained by varying l_2 . Light (set 1) and dark (set 2) curves correspond to the initial and modified designs, respectively. The simulated S_{11} parameter of the classical mushroom-like structure is shown in purple thick solid line. The horizontal dashed lines represent the phase criterion that the MTM must comply at 703–915 MHz to obtain constructive interference. The green colored bands show the frequencies in which the antenna must operate to cover all the specified uplinks.

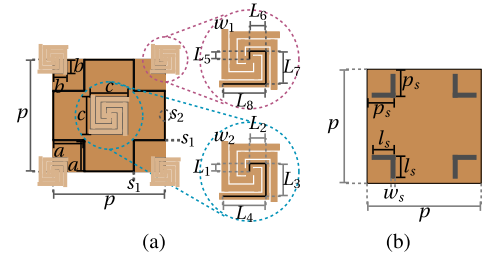


Fig. 6. Modified design of the UC of the MTM. The multilayered structure remains unaltered. (a) Top view (capacitive metasurface). (b) Bottom view (ground plane).

relies on the use of acrylic supports to create a reliable air gap l_2 . Nevertheless, we have considered possible errors in the construction stage and, accordingly, we performed a sensibility test in ANSYS HFSS by varying l_2 while keeping $W = 12$ mm and $g = 0.1$ mm. The result of this analysis is summarized in the set of light curves of Fig. 5, which gives the phase of the S_{11} parameter of the MTM alone [i.e., phase $\Phi(f)$ in (1)]. For completeness, we also show with a thick solid purple line the S_{11} parameter of the classical mushroom-like structure with $W = 60$ mm, $l_1 = 1.5$ mm and $g = 0.1$ mm. When $l_2 = 5$ mm, the fractional bandwidth of the proposed structure is 15.38%, approximately seven times the one that can be achieved with the classical mushroom-like structure in the same substrate. Despite this excellent result, this initial design has two main disadvantages. The first is that $\Phi(f)$ is sensitive to the air gap size. The second is that it is difficult to tune the central frequency by changing the free variables (capacitive gap and UC size). Fortunately, these problems can be overcome with a few changes. We have incorporated spiral inductors in the capacitive layer and slot inductors in the ground plane, as shown in Fig. 6. The spiral and slot inductors help in miniaturizing the design and also have the additional advantage of allowing an easy tuning of the central frequency by increasing the number of degrees of freedom. One disadvantage of the use of inductors in series is that it decreases the fractional bandwidth. This situation can be compensated, however, by increasing the air gap to 10 mm.

The simulated value of $\Phi(f)$ of the final design is shown in the second set of curves (dark lines) of Fig. 5. They show that the improved design can achieve a fractional bandwidth of 28.6%, which is better than required. The design parameters of the modified MTM UC are shown in Table I.

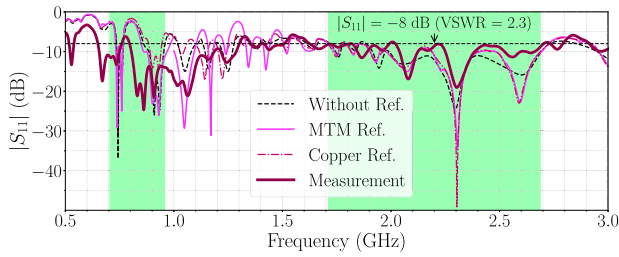


Fig. 7. Simulated S_{11} parameter of the radiator alone and integrated with a copper and an MTM reflector. The measured S_{11} parameter of the radiator integrated with the MTM is also shown (thick solid line).

C. Integration of the Radiator With the MTM Reflector

The complete MTM structure was simulated in conjunction with the radiator to ensure proper functionality. Simulations of the S_{11} parameter, radiation efficiency, and gain were done with ANSYS HFSS. We have simulated the antenna conductors with copper in order to obtain more realistic results. The frequency sweep of S_{11} was done with an interpolating sweep, while the simulations of efficiency and gain were done with a discrete sweep. Due to the high complexity of the design and the broadband and multiresonance characteristics, the simulation was partitioned in four frequency intervals, 0.5–0.8, 0.8–1, 1–1.5, and 1.5–3 GHz.

The simulated S_{11} parameters of the radiator without reflector, integrated with a copper reflector and with the MTM reflector are shown in Fig. 7. At high frequencies (greater than 1.7 GHz), the antenna has similar performance, both when it is integrated with the MTM reflector or the copper reflector. This behavior is expected, since the MTM was designed to behave as an EC at high frequencies. At low frequencies (less than 1 GHz) the antenna integrated with the MTM has better fractional bandwidth and more pronounced resonances, showing the better performance of the MTM reflector in comparison with its EC counterpart. It has to be noted that, due to the large computational cost required, the simulation did not converge at all frequencies.

The simulated radiation efficiency and gain are shown in Fig. 8. The MTM reflector presents better performance than the EC reflector in the lower part of the band, while in the upper part both performances are similar. We can also appreciate a region between 1.1 and 1.3 GHz where the MTM reflector has poor performance. This degradation is produced by a surface wave that propagates with losses through the MTM, which is verified by two characteristics. First, the radiation pattern is distorted and nearly omnidirectional at those frequencies and, second, by the increase in the magnitude of the electric field in the MTM. It has to be noted that the total power received by the antenna is quantified by the radiation efficiency (or gain) together with the S_{11} parameter. Considering a worst case scenario of $S_{11} = -8$ dB, the radiation efficiency should be corrected by a factor of 0.84 and the gain by 0.76 dB.

IV. MEASUREMENTS AND DISCUSSION

To validate the theoretical structure and the predicted performance, we constructed and tested a single-element antenna and a 2×2 array.

A. Single-Element Antenna

The prototype single-element antenna is shown in Fig. 9(a). The FR4 laminates and the radiator are mechanically assembled with acrylic supports and nylon screws. Scattering parameter measurements at the input port were made with a vector network analyzer,

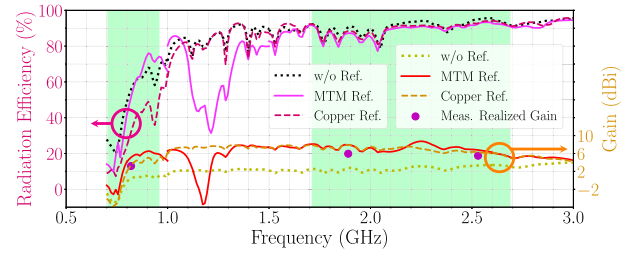


Fig. 8. Simulated radiation efficiency and total gain at $\theta = 0^\circ$ (normal to the plane of the radiator) of the radiator without reflector, integrated with a copper reflector and integrated with an MTM reflector. The measured total realized gain at $\theta = 0^\circ$ is shown with purple dots.

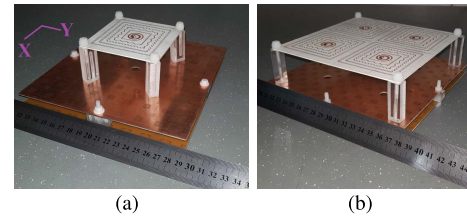


Fig. 9. Picture of the fabricated antennas. (a) Single-element antenna. (b) 2×2 array. In both cases the MTM reflector has a size of 18 cm \times 18 cm.

while radiation pattern and gain measurements were made with a far-field beam scanner.

Fig. 7 shows the simulated and measured S_{11} parameters. The measured S_{11} parameter is less than -8 dB in the bands 650–760, 790–1300, and 1620–2790 MHz, covering all the specified UMTS/LTE bands. The main differences between measurement and simulation are in the range 500–1000 MHz. These differences are due to the large computational cost required at those frequencies. In fact, at lower frequencies the HFSS simulation did not converge properly.

The measured and simulated beam patterns in two orthogonal planes are shown in panels (a)–(c) of Fig. 10. Since the spiral antenna is elliptically polarized, we have measured the gain in two orthogonal linear polarizations. We have selected 820, 1890, and 2530 MHz as representative frequencies from the specified uplinks. The measured front-to-back ratio at 820 MHz is 8.5 dB in the Y-pol and 5.8 dB in the X-pol. Although these values are not as high as required for some applications, this can be improved by increasing the size of the reflector. Indeed, the size of 18 cm is less than $\lambda/2$ at 820 MHz, whilst a good reflector should have a size of the order of λ . A simulation with a reflector size of 24 cm shows an improvement of 4.7 dB in the front-to-back ratio at 820 MHz. The measured total realized gain is shown in Fig. 8 for the three aforementioned frequency points. It can be seen that the measured realized gain is comparable with the simulated total gain within an acceptable range (given by the 0.76 dB correction factor of the reflections, and the measurement and simulation errors).

Phased arrays should have a field of view (maximum synthesized beam tilt angle without grating lobes) greater than $\pm 30^\circ$ to be useful in a wide range of applications. Therefore, the radiating elements must have a size smaller than 0.65 times the wavelength at the higher frequency [5], so that they can be closely spaced in the array. This fact, and the comparison with other recent broadband/multiband antennas (Table II) sheds light on the excellent performance of the antenna presented in this work. In particular, it has small dimensions, both at the minimum frequency that satisfies $S_{11} < -8$ dB and at the one that satisfies gain > 3 dBi. Since the proposed antenna

TABLE II
COMPARISON BETWEEN THE PROPOSED ANTENNA AND OTHER RECENT BROADBAND/MULTIBAND ANTENNAS

Reference	Antenna type		Radiator maximum dimension* λ_{\max}	Freq. range with $ S_{11} < -8$ dB		Freq. range with gain > 3 (or 0) dBi**		Max gain dBi	Half-space radiation [‡]	Suitable for wideband phased arrays ^{††}
	Radiator	Reflector		MHz	Fractional	MHz	Fractional			
This work	Meandered spiral	MTM	0.20	650-760 & 790-1300 & 1620-2790	16% & 49% & 53%	780-1120 & 1200-3000	36% & 86%	8.7	Yes	Yes
[8]	Meandered spiral	No	0.40	430-1500	111%	680-1340	65%	3.9	No	No
[10]	UWB Monopole	MTM	0.22	2200-2600 & 4080-6500	17% & 46%	2190-2810 & 4780-6220	25% & 26%	7	Yes	No
[11]	Crossed dipoles	MTM	0.46	1150-2300	67%	1100-1870	52%	6	Yes	No
[12]	Aperture antenna	MTM	0.59	4900-7350	40%	4600-7000	41%	7	Yes	No
[13]	Patch antenna	MTM	0.60	4500-8000	56%	4000-7100	56%	6.5	Yes	No
[15]	Archimedean spiral	MTM	N/A	N/A	N/A	5000-6400	25%	9	Yes	No
[18] ^{‡*}	Four-Armed spiral	No	0.33	500-3500	150%	750-3500	129%	5.8	No	No
[19]	Meandered and resistive-loaded conical spiral	No	0.32	200-1000	133%	550-1000	58%	5	Yes	No
[20]	Equiangular spiral	Cavity backed	0.88	2000-14500	152%	4700-18000	117%	4	Yes	No
[21] ^{‡*}	Four-armed helix-spiral	EC	0.34	200-2600	171%	640-2600	121%	9	Yes	No
[22]	Antipodal Vivaldi	No	0.41	1300-17000	172%	1300-17000	172%	9.3	Yes	No

*Maximum lateral dimension of the radiator with respect to the minimum frequency that satisfies both $S_{11} < -8$ dB and gain > 3 dBi.

**3 dBi if the antenna has half-space radiation and 0 dBi otherwise.

‡Considering an unique mainlobe.

††Considering broadband or multiband applications with $f_{\max} > 3f_{\min}$ (such as the separation given in the LTE and UMTS uplinks), being f_{\max} and f_{\min} the max. and min. frequencies that satisfy both $S_{11} < -8$ dB and gain > 3 dBi. The electrical size should be less than 0.65 times the wavelength at the higher frequency.

‡*Requires 4 input ports with 90° phase differences between each.

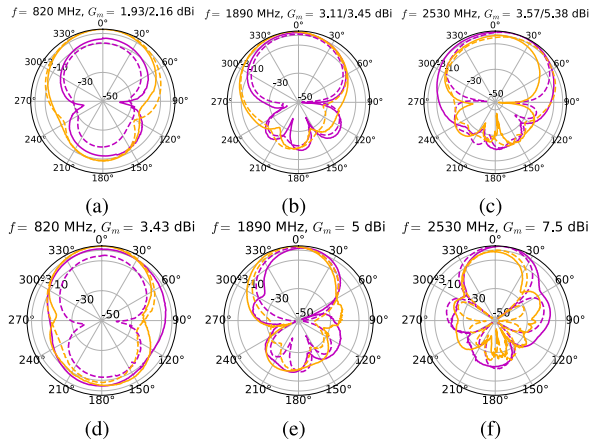


Fig. 10. Measured (solid lines) and simulated (dashed lines) radiation patterns of the single-element antenna (a)–(c) and the antenna array (d)–(f) in decibel. Purple lines correspond to the X-pol while orange lines correspond to the Y-pol (the X and Y coordinates are defined in Fig. 9). (a) Measurements are normalized with respect to their maximum (left value of G_m) and simulations are normalized with respect to their maximum (right value of G_m). Array measurements only show the measured maximum value. (a) and (d) 820 MHz. (b) and (e) 1890 MHz. (c) and (f) 2530 MHz.

satisfies these characteristics simultaneously, it can be integrated into wideband arrays with half-space radiation.

B. 2×2 Array

Based on the single-element antenna, a 2×2 array was studied experimentally. A picture of the array is shown in Fig. 9(b). The distance between elements is 7.5 cm, which enables a field of view of 67° at 2570 MHz and a complete field of view in all the uplinks below 2 GHz. The measured reflections of the four antennas of the array are shown in Fig. 11. The measurements show differences between each individual element of the array at lower frequencies. This discrepancy can be explained by the fact that the currents at those frequencies are concentrated in the outer regions of the spirals, and thus are more affected by the position of each element within the array. The coupling among the antennas (not shown) is lower than -10 dB from 500 to 3000 MHz.

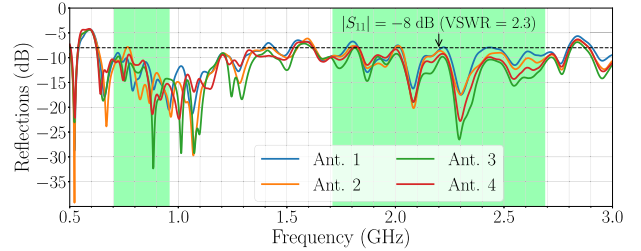


Fig. 11. Measured reflections of each element of the 2×2 array.

The measured array beam patterns in two orthogonal planes and two orthogonal polarizations are shown in panels (d)–(f) of Fig. 10. The array could not be simulated in HFSS due to the high computational cost required. However, to characterize how the coupling affects the radiation patterns, we have plotted in dashed lines the measured single-element antenna gains multiplied by the theoretical array factors. It can be seen that the measured gain presents higher sidelobes than expected at 1890 and 2530 MHz, which could be attributed to the coupling. However, the sidelobe level is still below -10 dB with respect to the maximum.

V. CONCLUSION

A multiband antenna, suitable as an array element has been designed, built, and characterized. It consists of a miniaturized Archimedean spiral antenna integrated with an MTM reflector. The single-element antenna has an S_{11} parameter smaller than -8 dB in the 650–760 MHz, 790–1300 MHz, and 1620–2790 MHz frequency bands. The radiator has a size of 7.5 cm, allowing compact array applications. This low separation between elements enables the synthesis of an array factor without grating lobes from 700 to 2000 MHz. The MTM reflector has demonstrated a better performance than the common EC reflector, as it gives a higher radiation efficiency in the frequency bands of interest. This behavior has been achieved by using it in a nonconventional way, as AMC in part of the band, and as EC otherwise.

The combination of characteristics of the antenna presented in this work (small size, half-space radiation, broad impedance

bandwidth, and high efficiency) make it outstanding among other recent antennas developed for similar frequency ranges. In particular, its characteristics convert this antenna into an excellent candidate for multiband antenna arrays.

REFERENCES

- [1] H. Chen and A. Zhao, "LTE antenna design for mobile phone with metal frame," *IEEE Antennas Wireless Propag. Lett.*, vol. 15, pp. 1462–1465, 2015, doi: [10.1109/LAWP.2015.2513078](https://doi.org/10.1109/LAWP.2015.2513078).
- [2] J. Kaiser, "The archimedean two-wire spiral antenna," *IRE Trans. Antennas Propag.*, vol. 8, no. 3, pp. 312–323, May 1960, doi: [10.1109/TAP.1960.1144840](https://doi.org/10.1109/TAP.1960.1144840).
- [3] C. Jarufe *et al.*, "Optimized corrugated tapered slot antenna for mm-wave applications," *IEEE Trans. Antennas Propag.*, vol. 66, no. 3, pp. 1227–1235, Mar. 2018, doi: [10.1109/TAP.2018.2797534](https://doi.org/10.1109/TAP.2018.2797534).
- [4] F. Fereidoony, S. Chamaani, and S. A. Mirtaheeri, "Systematic design of UWB monopole antennas with stable omnidirectional radiation pattern," *IEEE Antennas Wireless Propag. Lett.*, vol. 11, pp. 752–755, 2012, doi: [10.1109/LAWP.2012.2205658](https://doi.org/10.1109/LAWP.2012.2205658).
- [5] W. L. Stutzman and G. A. Thiele, *Antenna Theory and Design*. Hoboken, NJ, USA: Wiley, 2013.
- [6] K. Fujimoto and H. Morishita, *Modern Small Antennas*. New York, NY, USA: Cambridge Univ. Press, 2013.
- [7] B. A. Kramer, C.-C. Chen, and J. L. Volakis, "Size reduction of a low-profile spiral antenna using inductive and dielectric loading," *IEEE Antennas Wireless Propag. Lett.*, vol. 7, pp. 22–25, 2008, doi: [10.1109/LAWP.2007.914116](https://doi.org/10.1109/LAWP.2007.914116).
- [8] T.-Y. Shih and N. Behdad, "A miniaturized, ultra-wideband, circularly polarized spiral antenna," in *Proc. Int. Workshop Antenna Technol., Small Antennas, Novel EM Struct. Mater., Appl. (iWAT)*, Mar. 2014, pp. 328–331, doi: [10.1109/IWAT.2014.6958678](https://doi.org/10.1109/IWAT.2014.6958678).
- [9] D. Sievenpiper, "High-impedance electromagnetic surfaces," Ph.D. dissertation, Dept. Elect. Eng., Univ. California at Los Angeles, Los Angeles, CA, USA, 1999.
- [10] M. Ameen, V. R. Ramireddy, and R. K. Chaudhary, "A compact dual-band and dual-polarized open-ended ZOR antenna with AMC ground plane for 4G-LTE/WLAN/WiMAX applications," in *Proc. IEEE Indian Conf. Antennas Propog. (InCAP)*, Dec. 2018, pp. 1–4, doi: [10.1109/INCAP.2018.8770831](https://doi.org/10.1109/INCAP.2018.8770831).
- [11] D. Feng, H. Zhai, L. Xi, S. Yang, K. Zhang, and D. Yang, "A broadband low-profile circular-polarized antenna on an AMC reflector," *IEEE Antennas Wireless Propag. Lett.*, vol. 16, pp. 2840–2843, 2017, doi: [10.1109/LAWP.2017.2749246](https://doi.org/10.1109/LAWP.2017.2749246).
- [12] K. Agarwal, K. Nasimuddin, and A. Alphones, "Wideband circularly polarized AMC reflector backed aperture antenna," *IEEE Trans. Antennas Propag.*, vol. 61, no. 3, pp. 1456–1461, Mar. 2013, doi: [10.1109/TAP.2012.2227446](https://doi.org/10.1109/TAP.2012.2227446).
- [13] T. Nakamura and T. Fukusako, "Broadband design of circularly polarized microstrip patch antenna using artificial ground structure with rectangular unit cells," *IEEE Trans. Antennas Propag.*, vol. 59, no. 6, pp. 2103–2110, Jun. 2011, doi: [10.1109/TAP.2011.2143656](https://doi.org/10.1109/TAP.2011.2143656).
- [14] H. Nakano, K. Kikkawa, N. Kondo, Y. Iitsuka, and J. Yamauchi, "Low-profile equiangular spiral antenna backed by an EBG reflector," *IEEE Trans. Antennas Propag.*, vol. 57, no. 5, pp. 1309–1318, May 2009, doi: [10.1109/TAP.2009.2016697](https://doi.org/10.1109/TAP.2009.2016697).
- [15] H. Nakano, K. Hitosugi, N. Tatsuzawa, D. Togashi, H. Mimaki, and J. Yamauchi, "Effects on the radiation characteristics of using a corrugated reflector with a helical antenna and an electromagnetic band-gap reflector with a spiral antenna," *IEEE Trans. Antennas Propag.*, vol. 53, no. 1, pp. 191–199, Jan. 2005, doi: [10.1109/TAP.2004.840755](https://doi.org/10.1109/TAP.2004.840755).
- [16] C. Djoma, "Maximal bandwidth of an archimedean spiral antenna above a reflector," *IEEE Antennas Wireless Propag. Lett.*, vol. 13, pp. 333–336, 2014, doi: [10.1109/LAWP.2014.2303858](https://doi.org/10.1109/LAWP.2014.2303858).
- [17] D. Gallardo, "Diseño, construcción y caracterización de un arreglo de antenas de Banda ancha basado en metamateriales," M.S. Thesis, Dept. Elect. Eng., Univ. Chile, Santiago, Chile, 2020. [Online]. Available: <http://repositorio.uchile.cl/handle/2250/176925>
- [18] D. Li, L. Li, Z. Li, and G. Ou, "Four-arm spiral antenna fed by tapered transmission line," *IEEE Antennas Wireless Propag. Lett.*, vol. 16, pp. 62–65, 2017, doi: [10.1109/LAWP.2016.2555839](https://doi.org/10.1109/LAWP.2016.2555839).
- [19] H.-S. Youn, N. Celik, M. Iskander, J. Baker, J. Graham, and S. Murphy, "Miniaturized conical spiral antenna with tapered resistive loading and corrugated arms," in *Proc. IEEE Int. Symp. Antennas Propag. (APSURSI)*, Jul. 2011, pp. 1185–1188, doi: [10.1109/APS.2011.5996496](https://doi.org/10.1109/APS.2011.5996496).
- [20] C. M. Seong and D. C. Park, "Design of cavity-backed spiral antennas," *Proc. 5th Global Symp. Millim.-Waves*, 2012, pp. 1–5, doi: [10.1109/GSMM.2012.6314032](https://doi.org/10.1109/GSMM.2012.6314032).
- [21] M. J. Radway and D. S. Filipovic, "Four-armed spiral-helix antenna," *IEEE Antennas Wireless Propag. Lett.*, vol. 11, pp. 338–341, 2012, doi: [10.1109/LAWP.2012.2191384](https://doi.org/10.1109/LAWP.2012.2191384).
- [22] Z. Wang, Y. Yin, J. Wu, and R. Lian, "A miniaturized CPW-fed antipodal vivaldi antenna with enhanced radiation performance for wideband applications," *IEEE Antennas Wireless Propag. Lett.*, vol. 15, pp. 16–19, 2016, doi: [10.1109/LAWP.2015.2425735](https://doi.org/10.1109/LAWP.2015.2425735).